[redacted] STRUCTURE AND UTILIZATION OF SUPERSONIC FREE JETS IN LOW DENSITY WIND TUNNELS[1]

by

Harry Ashkenas
Jet Propulsion Laboratory, Pasadena

and

Frederick S. Sherman
University of California, Berkeley

I. INTRODUCTION

At the Rarefied Gas Dynamics Symposium of 1962, considerable attention was drawn to the process of unconfined expansion from a sonic orifice into a low pressure chamber as an effective means of obtaining high Mach number flows of very low density gases. These "free jet" flows were discussed in the context of aerodynamically-intensified molecular beam sources (Bier and Hagena, (1963), (Fenn and Deckers, (1963), and were suggested as a useful supplement to conventional nozzle-confined expansions for some classes of wind tunnel tests (Sherman, (1963a). They had also been extensively studied in connection with aerodynamic schemes of isotope separation (Zigan, (1962).

In the last two years, interest in these flows has intensified, and considerable progress has been made toward their accurate description, as function of the pressure ratio across the orifice, the specific-heats-ratio of the gas, and the orifice Reynolds number. Groups at both the University of California at Berkeley and the Jet Propulsion Laboratory in Pasadena have been working actively and in a complementary fashion on this problem, and because of the proximity of the two groups, a joint report of our results was deemed feasible.

[1]This paper presents the results of one phase of research carried out at the Jet Propulsion Laboratory, California Institute of Technology, under Contract No. NAS 7-100, sponsored by the National Aeronautics and Space Administration, and at the University of California under Contract Nonr-222(45), sponsored by the Office of Naval Research and the Office of Scientific Research. [redacted]

Our aim is to give a concise and easily-employed guide to the results of the theory of inviscid and slightly-viscous flow in the central core of the jet, a resume and confirmation of experimental results concerning the location of shock waves at high Reynolds number; an application of this information to prediction of the jet sizes and the Mach and Reynolds number ranges corresponding to various pumping systems; and a preliminary experimental description of the manner in which the jet flow itself undergoes transition from an inviscid-continuum flow to a free-molecular flow as the orifice Reynolds number decreases. Another paper at the symposium (Maslach, et. al., (1964) will report a successful application of the free jet flow in a determination of cylinder and strip drag in the near-free-molecule regime.

II. RESULTS OF INVISCID FLOW THEORY

The transonic inviscid flow through a circular hole in a thin wall, or through a rapidly converging axisymmetric nozzle, presents an unsolved problem in potential flow theory. However, the details of flow in the transonic region evidently have little influence in the region more than a nozzle diameter downstream, and successful treatments of the supersonic region have been based on the assumption that flow in the plane of the orifice or nozzle exit is uniform and slightly supersonic. The method of characteristics may then be applied, yielding accurate flow data at a number of discrete mesh points.

Owen and Thornhill (1952) were the first to carry out such a computation, and for many years their solution has been the only standard of comparison for experimentalists. Computer programs more than adequate for the task have been in existence in many organizations for several years, but have been applied to much more complicated problems, exemplified by the work of Love, et. al. (1959). The computations used in this paper were performed in 1962 by W. S. Woolff of the Lockheed Missiles and Space Company in Palo Alto, using a program which is capable of finding the jet boundary and the barrel shock location, almost up to the point of Mach intersection. They assumed a perfect gas with constant specific heats (γ = 1.67, 1.40, or 1.2857), and uniform exit flow at a Mach number of 1.10.

A. Centerline Property Distributions

1. The High Supersonic Region

The computed free jet flows exhibit a relatively simple and self-similar development in the inertia-dominated region of high Mach number isentropic flow, inside the barrel shock (see Fig. 1). There the streamlines appear to radiate from a "source" at a distance x_0 (measured in orifice radii) downstream of the orifice, the flow speed has very nearly attained its adiabatic-flow limit, and density decreases along each streamline in proportion to the inverse square of distance from this source. The variation of density from streamline to streamline (i.e., with polar angle θ, at constant distance, R, from the "source") is approximately independent of R. These facts are commented on in a preliminary way in an earlier unpublished report (Sherman, (1963b), a more finished version of which is hopefully forthcoming (Sherman, (1964a).

a. Mach number. The analogy to a "simple" (purely radial) source flow is strong, and suggested the following extremely accurate fitting formula for the centerline Mach number of a free jet:

$$M = A\left(\frac{x - x_0}{D}\right)^{\gamma-1} - \frac{1}{2}\left(\frac{\gamma + 1}{\gamma - 1}\right)\left[A\left(\frac{x - x_0}{D}\right)^{\gamma-1}\right]^{-1} \qquad (1)$$

The constants A and x_0 depend upon γ. A preliminary value of x_0 was found by projecting streamlines back to the axis. The final values were found as follows.

For a chosen value of x_0, Eq. (1) is solved for

$$A = \frac{M + \left[M^2 + 2\left(\frac{\gamma + 1}{\gamma - 1}\right)\right]^{1/2}}{2\left(\frac{x - x_0}{D}\right)^{\gamma-1}}$$

Values of M and x/D are inserted from the characteristics solution, and if the value of x_0 is good, the same value of A (except only for a small random scatter due to mesh-size errors in the characteristics computation) results for all values of $M > 5.5$, a value which indicates the threshold of

the inertia-dominated region. If this does not happen at first, x_0 is adjusted until it does. The final values in Table 1 cause Eq. (1) to reproduce the computer data in this region within this random scatter, the maximum deviations being about 1/2% of M.

It is tempting to continue Eq. (1) with a third term of the form

$$C\left(\frac{x - x_0}{D}\right)^{-3(\gamma-1)} ,$$

and indeed values of C can be found which give an accurage data fit, extending upstream to surprisingly small values of x/D. These values are included in Table 1, but with the explicit warning that the scatter in the computer data precludes any definite conclusion as to the correctness of the analytic form of this last term.

b. Impact pressure. Since impact pressure is the easiest quantity to obtain experimentally, we give explicit fitting formulas for it in the form

$$\frac{p_i}{p_0} = \left(\frac{\gamma + 1}{\gamma - 1}\right)^{\gamma/\gamma-1}\left(\frac{\gamma + 1}{2\gamma}\right)^{1/\gamma-1} A^{-2/\gamma-1}\left(\frac{x - x_0'}{D}\right)^{-2} \qquad (2)$$

While in principle the constant x_0' should be the same as x_0 of Eq. (1), we can improve the impact pressure prediction at small x, (without harming it at large x), by readjusting x_0' as shown in Table 1. The resulting formula gives 1 percent or better prediction of the characteristics data for $x/D \geq 2.5$ for all γ.

2. The Transonic Region. Effects of Entry Shape.

The assertion made above about the weak reliance of the flow in the high supersonic region upon the details of the transonic exit conditions was verified experimentally at Berkeley. The centerline static pressure was measured with a 0.300 inch diameter tube on the axis of a 3.00 inch diameter nozzle. The nose of the tube was always in the stagnation chamber and the static pressure taps were 13 inches aft of the nose and 14 inches upstream of the support. The tests compared the flow through a thin-plate (1/16 inch thick) orifice with that through a gradually

converging nozzle with a 0.9 inch long constant diameter throat section. They covered the region in which $0.05 \leq M \leq 4$, for nozzle Reynolds numbers of 7,960; 2,660; and 690. Mach numbers deduced by isentropic flow assumption at these Reynolds numbers agreed internally within 1 percent for a given geometry, there being a very slight systematic trend toward higher Mach number with decreasing Reynolds number.

Results for the two geometries are compared in Fig. 2. They come together very quickly as x/D exceeds about 1/2. The small residual difference for $x/D > 1/2$, between the results for the two entry shapes and the theoretical result for uniform exit flow at $M \simeq 1.10$, can be effectively removed by assigning an "effective diameter," D*, to the nozzle or orifice, which is slightly smaller than the diameter of the uniform flow section assumed for the theory. For the nozzle $D^*/D = 0.975$; for the orifice $D^*/D = 0.935$. As will be discussed later, D* may decrease further with decreasing Reynolds number, but the values cited here are thought to be characteristic of essentially inviscid flow.

B. Angular Variation of Flow Properties in the Inertia-Dominated Region

The approximately self-similar behavior of the density field, and hence the impact pressure field, in the inertia-dominated region consists in ρR^2 being only a function of θ. When ρR^2 was computed for a large number of points selected from the data of the method-of-characteristics calculation, they exhibited considerable scatter, but could be fitted by the simple formula

$$\frac{\rho(R, \theta)}{\rho(R, 0)} = \cos^2\left(\frac{\pi\theta}{2\phi}\right) \tag{3}$$

with an accuracy of about 3 percent of $\rho(R, 0)$. The constant ϕ depends on specific heats ratio as shown in Table 1.

This formula, and its counterpart

$$\frac{\rho(r, x)}{\rho(o, x)} = \cos^2\theta \cos^2\left(\frac{\pi\theta}{2\phi}\right) \tag{4}$$

are sufficiently accurate for such purposes as the correction of aerodynamic drag data for radial variation of dynamic pressure (Tang, (1964), (Ko, 1964) (the speed u is essentially constant in the inertia-dominated region) but the suggested analytic form is almost certainly not theoretically significant. In particular, it gives a value of $\partial^2\rho/\partial\theta^2$ at $\theta = 0$ which is inconsistent with the centerline Mach number distribution given by Eq. (1). This point will be further elucidated by Sherman (1964a).

C. Experimental Verification of the Inviscid Theory

Some of the earliest quantitative data on free jet structure were obtained by interferometric techniques by Landenburg, et. al. (1949). Owen and Thornhill (1948) cited a successful comparison of their theory with impact pressure data of Hartmann and Lazarus (1941). A recent extensive study using impact pressure and mass flow probes was made by Reis (1962) and a considerable body of data has been accumulated by the present authors and their coworkers. Samples of impact pressure data on the jet centerline and in various cross sections normal to the axis are shown in Figs. 3 and 4.

In general, there seems to be no difficulty in obtaining impact pressure data which are in excellent accord with theory if due care is taken to have the probe not too large (thereby incurring probe "displacement" effects), nor too small (necessitating a probe calibration for probe viscous effects), nor too highly yawed.

III. SHOCK WAVE CONFIGURATIONS IN NEARLY INVISCID FLOW

For a given specific heats ratio, the shape and size of the barrel shock and Mach disc are determined by the pressure ratio across the orifice or nozzle. A comprehensive photographic study was made by Bier and Schmidt (1961) covering a wide range of pressure ratios and a variety of monatomic, diatomic and triatomic gases. We have checked their results for axial distance to the Mach disc by impact pressure and free-molecule wire techniques and find that

$$\frac{x_M}{D} = 0.67\left(\frac{p_0}{p_1}\right)^{1/2} \qquad (5)$$

independent of the value of γ, for $15 \leq p_0/p_1 \leq 17,000$. Our data are shown in Fig. 5. The scatter which is evident arises in determinations of the "location" of rather thick shocks, in which an attempt was made to identify the center of a broad impact pressure "dip" attributed to the structure of the shock.

A relation of the form of Eq. (4) was predicted by Adamson and Nicholls (1959), who argued that the static pressure behind the Mach disc would be about equal to the test chamber pressure. A similar argument might be advanced for the impact pressure behind the shock, and we indeed find p_{i_M}/p_1 to be very nearly independent of p_0/p_1, a fact which is useful in the planning of experiments in the free jet, and in estimating conditions just upstream of the Mach disc. Our data are shown in Fig. 6.

Bier and Schmidt (1961) also measured the maximum diameter of the barrel shock and the Mach disc diameter as a function of p_0/p_1. They found, for air,

$$D_M/x_M = 0.42 \text{ and } 0.48 \text{ at } p_0/p_1 = 20 \text{ and } 1000.$$

Corresponding ratios are about 25 percent larger for CO_2 ($\gamma = 9/7$) and about 20 percent smaller for argon ($\gamma = 5/3$).

IV. VISCOUS EFFECTS IN FREE JETS

Viscous effects in the free jet are of four types:

1. boundary-layer growth on the converging nozzle, which can produce a change in effective orifice size and a distortion of the flow pattern near the orifice. This effect is seen in the variation of nozzle discharge coefficient with Reynolds number and in a shrinking of the scale of the flow downstream, and is generally very small if the nozzle Reynolds number is more than a few hundred.

2. mixing-layer growth at the free jet boundary. This has no effect on the flow inside the shock barrel until, under circumstances of low Reynolds number and high pressure ratio, the mixing layer begins to overlap with, and eventually to eradicate the downstream portions of the shock barrel and the Mach disc.
3. thickening of the shock waves that form the sides and bottom of the barrel. This, in combination with the growth of the mixing layer, is the most prominent qualitative feature of the observed transition from the typical nearly-inviscid flow pattern to free-molecular effusion, but it presumably does not influence the flow upstream of these shocks, as long as any such flow exists.
4. viscous dissipation, etc., in the "core" of the flow, arising from the slight but non-vanishing velocity and temperature gradients in that region. These effects may be of experimental significance at points on or near the jet axis and far downstream from the orifice, at Reynolds numbers so large that the first three classes of effects are insignificant.

A. Dissipation Effects in the Core

This last class of viscous effects, along with the thickening of the Mach disc, were investigated by Sherman (1964b) by use of a simple source-flow model. A result was a prediction of the minimum Reynolds number (based on sonic flow properties and the sonic sphere radius) which would permit the use of inviscid theory to specify the Mach number at a given radius within a certain small error. In particular, it was found that the Mach number perturbation is due almost entirely to a small amount of viscous dissipation, which depletes the directed kinetic energy only negligibly, but raises the internal energy significantly--a characteristic hypersonic effect.

The analysis made use of an "outer" expansion of all flow properties in asymptotic series in inverse integral powers of the Reynolds number, and an initial condition which assigned an inviscid value to the velocity at a fixed radius, slightly larger than the sonic radius.

With the perfect gas assumption, the expansion for velocity and temperature

$$\left.\begin{aligned} u &= u_0 + \left(\frac{1}{Re}\right)u_1 + \cdots \\ T &= T_0 + \left(\frac{1}{Re}\right)T_1 + \cdots \end{aligned}\right\} \tag{6}$$

can be combined with one for the Mach number

$$M = M_0\left[1 + \left(\frac{m_1}{Re}\right) + \cdots\right] \tag{7}$$

to show that

$$M_1 = \left(\frac{u_1}{u_0}\right) - \frac{1}{2}\left(\frac{T_1}{T_0}\right) , \tag{8}$$

where subscript zero denotes the inviscid approximation and subscript one the first viscous perturbation.

With a viscosity-temperature law, $\mu \alpha \quad T^{\omega}$, with constant ω, there followed the asymptotic result for large radius,

$$m_1 \sim \frac{-2\gamma(\gamma - 1)\left(\frac{\gamma + 1}{\gamma - 1}\right)^{1/2\left[\gamma+1-\omega(\gamma-1)\right]}\left(\frac{\lambda}{\mu} + 1\right)}{1 + 2(\gamma - 1)(1 - \omega)}\left(\frac{r}{r_*}\right)^{1+2(\gamma-1)(1-\omega)} \tag{9}$$

where μ and λ are the viscosity coefficients in the Navier-Stokes relation

$$\tau_{ij} = \mu\left(\frac{\partial u_i}{\partial x_j} + \frac{\partial u_j}{\partial x_i}\right) + \lambda \operatorname{div} \vec{u}\, \delta_{ij} \quad .$$

This asymptotic result is accurate for $M_0 \geq 7$ for $\gamma = 7/5$ and $M_0 \geq 10$ for $\gamma = 5/3$, at which values the contribution of u_1/u_0 to m_1 is quite negligible. Under these conditions we can readily show that $-m_1$ is

simply proportional to the entropy increase of the gas. This follows from the perfect gas relation,

$$\frac{dT}{T} = \frac{dS}{C_v} + (\gamma - 1)\frac{d\rho}{\rho} \quad , \tag{10}$$

and the continuity equation for the simple source flow,

$$\rho u r^2 = \text{const.} \tag{11}$$

Combining these equations and integrating to r from a radius r_1 at which the entropy is called zero, we get

$$\ell n T = \frac{S}{C_v} - (\gamma - 1)\ell n u - 2(\gamma - 1)\ell n r + \text{const.}$$

Expanding this in inverse powers of Re, and combining with the definition of m_1, we find

$$m_1 = -\frac{1}{2}\frac{S_1}{C_v} + \frac{\gamma + 1}{2}\frac{u_1}{u_0} \quad , \tag{12}$$

in which the second term on the right is negligible for large r.

This same approach can be carried over to the free jet itself, by use of the general continuity equation in place of $\rho u r^2$ = constant. Then we can combine (9) and (10) into

$$\frac{D(\ell n T)}{Dt} = \frac{D(S/C_v)}{Dt} - (\gamma - 1)\,\text{div}\,\vec{u} \quad ,$$

which may be integrated along the jet axis from a point in the plenum chamber to the point of observation. When the result is expanded in inverse powers of Re, we find

$$m_1 = -\frac{1}{2}\frac{S_1}{C_v} + \int_{-\infty}^{x}\left[\frac{d}{dx}\left(\frac{u_1}{u_0}\right) + \frac{\gamma - 1}{2}\frac{\operatorname{div}\vec{u}_1}{u_0} - \frac{\gamma - 1}{2}\frac{\operatorname{div}\vec{u}_0}{u_0}\frac{u_1}{u_0}\right]dx \qquad (13)$$

where u is the scalar speed along the axis. We shall now assume that for the large values of x (and high Mach numbers) of interest, the contribution of the integral on the right, which will be of order u_1/u_0, is negligible, and thus we use only

$$m_1 \doteq \frac{1}{2}\frac{S_1}{C_v} \quad . \qquad (14)$$

The entropy perturbation S_1 is readily calculated along the jet axis, if we are given the inviscid flow field. In fact, all that is needed is the distribution of M_0 versus x.

The basic equation employed is

$$S - S_0 = \int_{-\infty}^{x}(\Phi - \operatorname{div}\vec{q})\frac{dx}{\rho u T} \qquad (15)$$

where Φ is the viscous dissipation function and $\vec{q}$ the heat flux vector. We expand this in inverse powers of Re and assume that the inviscid flow near the axis can be represented by power series in distance from the axis. This gives such results, on the axis, as

$$\operatorname{div}\vec{u}_0 = M_0^2\frac{\partial u_0}{\partial x} \quad ,$$

and

$$\frac{\partial v_0}{\partial r} = \left(M_0^2 - 1\right)\frac{\partial u_0}{\partial x} \quad ,$$

(v and r are velocity and position components normal to the axis.)

Treating the Prandtl number, $Pr = \mu c_p/k$, as constant, we reduce Eq. (15) to a final form,

$$\frac{S - S_0}{C_v} = \int_{-\infty}^{x} \left\{ \frac{4\gamma(\gamma - 1)\left[\left(\frac{\lambda}{\mu} + 1\right)M^4 - 2M^2 + 3\right]}{\left[2 + (\gamma - 1)M^2\right]^2} \left(\frac{dM}{dx}\right)^2 \right.$$

$$\left. + \frac{\gamma}{Pr}\left[\frac{\nabla^2 T}{T} + \frac{\omega}{T^2}\left(\frac{dT}{dx}\right)^2\right] \right\} \frac{\mu\, dx}{\rho u} \quad . \tag{16}$$

In this $\omega = d(\ell n \mu)/d(\ell n\, T)$ may be treated as a function of T. The terms involving T can be expressed in terms of M.

We have integrated Eq. (16) for air, assuming $\lambda = 0$, $\gamma = 7/5$, $Pr = 3/4$, and employing the curves for unit Reynolds number versus Mach number, given in NACA Technical Report 1135, to determine $\rho u/\mu$. The cases shown in Fig. 7a are for stagnation temperatures of 50°F, 500°F and 1400°F, and use the centerline Mach number distribution for the thin-plate orifice.

It turns out that the heat conduction terms are relatively most important near the plane of the orifice, where they actually produce a negative net integrand in Eq. (16). For large x, these terms become negligible rather rapidly, and the dominant term in the integrand is the very first one, which is just the same as the dominant term in the simple source flow. Physically, this term represents viscous dissipation arising from the "hoop stresses" due to the lateral stretching of the expanding fluid particles. The corresponding asymptotic result for m_1 is

$$m_1 \sim -\frac{2\gamma(\gamma - 1)\left(\frac{\lambda}{\mu} + 1\right)A^{\frac{2\gamma}{\gamma-1} - 2\omega}}{1 + 2(\gamma - 1)(1 - \omega)} \left(\frac{\gamma + 1}{\gamma - 1}\right)^{\omega - \frac{(\gamma+1)}{2(\gamma-1)}} \left(\frac{x - x_0}{D}\right)^{1+2(\gamma-1)(1-\omega)} \tag{17}$$

which reduces to Eq. (15) when $A = \left[(\gamma + 1)/(\gamma - 1)\right]^{(\gamma+1)/4}$, the value for a simple source flow. Here we have assumed that ω approaches a constant limit < 1 as $x \to \infty$. For the Sutherland viscosity law, which is used in

NACA TR 1135, the limiting value of ω is 3/2, and m_1 eventually grows in proportion to $(x - x_0/D)^{2-\gamma}$. In practice, wind tunnel workers having to deal with flows expanded to very low temperatures often disregard the Sutherland law for very low temperatures, and extrapolate viscosity data along a line $\mu \propto T(\omega = 1)$, from the origin to the point of tangency with a linear μ - T plot of the Sutherland law (i.e., at about T = 111°K for air). This procedure would lead to an eventual linear growth of m_1 with x, and results which are quantitatively very different at large x, as seen in Fig. 7a. In this calculation, as in the reduction of high Mach number free jet data, some well-based method of viscosity prediction for low temperatures is sorely needed.

The curve for $m_1(x)$ can be employed for two types of useful predictions, (a) of the minimum orifice Re required if the inviscid theory is to be trusted for given accuracy in M, and (b) the maximum M which can be obtained at a given orifice Re. The latter prediction strains one's faith in a small perturbation theory, but is included because the calculations show that M_{max} is attained when m_1/Re is only about 0.2 to 0.3. Some results are shown for air in Fig. 7b.

B. Boundary Layer Effects in the Entry Section

The variation of effective orifice diameter with Reynolds number was investigated experimentally at the Jet Propulsion Laboratory for $13 < Re < 2500$, with a square-edged orifice of thickness $t = 0.0266\ D$. It was found that the experimental axial impact-pressure distribution, when corrected for probe viscous effects by calibration factors determined in a uniform nozzle flow, and for shock displacement effect, could be brought into agreement with the predictions of inviscid flow theory by the assumption of a D^*/D dependent upon Re. The results are presented graphically in Fig. 8. Similar effects of larger magnitude and qualitatively different Re-dependence are seen in the flows from gradually converging nozzles. In the opinion of the authors, this constitutes an advantage of the thin plate orifice for free-jet formation, since this geometry postpones the onset of one class of viscous effects to the lowest possible Reynolds number.

C. Thickening of Shock Waves and Mixing Layer

Little can be said theoretically about the dramatic process of shock and mixing-layer thickening, and the interaction between them as Reynolds number decreases. Experimental evidence to date is limited to impact pressure surveys and flow visualization studies.

Axial impact pressure surveys exhibit a broadening of the "dip" which we associate with the Mach disc. Since the upstream entry into this dip is very smooth it is very hard to detect the upstream beginnings of the Mach disc from impact pressure data.

Radial impact pressure surveys taken at JPL for air at $x/D = 6$ and $p_0/p_1 = 100$ are shown for a wide range of Re in Fig. 9. The ordinate is direct pressure transducer output, uncorrected for probe viscous or yaw effects. The peak impact pressure associated with the recompressed flow outside the shock barrel falls relative to the centerline pressure as Re decreases, and the residual peaks move slightly toward the axis as they are consumed by the mixing layer.

As suggested by Bier and Hagena (1963), an appropriate dimensionless criterion for the disappearance of the Mach disc and its neighboring barrel shock as recognizable entities is the approach toward unity of a Knudsen number based on Mach disc diameter and mean free path behind the Mach disc. The latter mean free path is very nearly equal to that of the gas in the test chamber, with pressure p_1 and temperature T_0. When we take the inviscid flow value for Mach disc diameter corresponding to the measured p_0/p_1, and form a Knudsen number, Kn, with it and the "test chamber mean free path," we find that the impact pressure peaks of the radial survey just ahead of the Mach disc vanish at $K_M = 0.1$, and the last visible recompression by the Mach disc in the flow photos vanishes at $K_M = 0.25$.

V. APPLICATION OF FREE JETS AS WIND TUNNEL STREAMS

A. Attainable Jet Size

The distance x_M turns out, under reasonable assumptions, to be a simple measure of the volumetric capacity of the wind tunnel pumping plant. Suppose the pumps will handle a mass flow rate $\dot{m}$ at a suction

pressure equal to the test chamber pressure p_1. The stagnation temperature is T_0. Then

$$x_M = 0.75 \frac{(RT_0)^{\frac{1}{4}}}{\gamma} \left(\frac{\gamma + 1}{2}\right)^{\frac{1}{4}\left(\frac{\gamma+1}{\gamma-1}\right)} \left(\frac{\dot{m}}{p_1}\right)^{\frac{1}{2}}$$

For the No. 4 Wind Tunnel at the University of California, x_M turns out to be 11 to 14 inches, the variation being due to the non-linearity of the ($\dot{m}$ vs p_1) pump curve. For the Jet Propulsion Laboratory low density wind tunnel x_M is about 6 inches. The relationship above is quite accurate if $p_0/p_1 \geq 15$ and if the boundary layer thickness in the nozzle throat is only a small fraction of the nozzle radius.

B. Available Mach and Reynolds Number Ranges

The roughest outline of available Mach and Reynolds number range is obtained by fixing T_0 and then determining the boundaries corresponding (a) to a minimum test chamber pressure, $p_{1_{min}}$ and (b) to a maximum plenum chamber pressure, $p_{0_{max}}$. Then we fix attention on conditions just upstream of the Mach disc, which is the most desirable test region. Simple arguments, assuming isentropic flow in the core, lead to

(a)
$$\frac{Re_s}{L} = \frac{1.35\, p_1 \left(\frac{\gamma - 1}{2}\right)^{\omega}}{\left(\frac{2}{\gamma - 1} RT_0\right)^{\frac{1}{2}} \mu(T_0)} M_s^{2\omega}$$

for which we have assumed $\mu(T)/\mu(T_0) = (T/T_0)^{\omega}$.

$$\frac{Re_s}{L} = \frac{1.10\, p_0 \left(\frac{\gamma - 1}{2}\right)^{\omega}}{\left(\frac{2}{\gamma - 1} RT_0\right)^{\frac{1}{2}} \mu(T_0)} \left(\frac{\gamma + 1}{\gamma - 1}\right)^{\frac{\gamma}{\gamma-1}} \left(\frac{\gamma + 1}{2\gamma}\right)^{\frac{1}{\gamma-1}} M_s^{2\left(\omega - \frac{1}{\gamma-1}\right)}$$

These boundaries are sketched in Fig. 10 for the University of California, Berkeley No. 4 wind tunnel, for which we take $p_{1_{min}} = 0.060$ torr, $p_{0_{max}} = 1$ atmosphere, $T_0 = 300°K$, and consider air to have $\omega = 3/4$, and for the Jet Propulsion Laboratory Leg 1 tunnel, $p_{1_{min}} = 0.002$ torr.

Actually, this view of things may be quite oversimplified if p_1 is very low, or if $\dot{m}/p_1$ is small. Another low-pressure boundary criterion is set by the desire to have negligible viscous effects in the core of the jet.

The viscous flow analysis of Section III has been applied to draw into Fig. 10 curves for $m_1/Re_* = 0.05$, again with $\omega = 3/4$. If the Sutherland law is used, a curve results for this boundary, which imprcves the prospects for nearly inviscid flow at high M.

The criterion $K_m = 0.1$, indicating the total collapse of the inviscid flow picture in the vicinity of the Mach disc, is also indicated in Fig. 10. By virtue of the relation of jet dimensions to pumping speed, this criterion reduces to a fixed value of p_1 for a given pumping plant. For Berkeley, with $D_M \simeq 5.3$ inches, $p_1 = 3.8$ microns, an order of magnitude lower than the p_1 attainable with the steam ejectors. For JPL, $D_M = 2.9$ inches, $p_1 = 6.9$ microns, well within the available range.

The high pressure limit ($p_{0_{max}} = 1$ atmosphere) may also be too approximate, because of the possibility of condensation of the air components. We are currently investigating this experimentally, and have been unable to isolate any condensation effects on impact pressure data, even when expanding from the S. T. P. conditions to a Mach number of 22!

C. Effect of Stagnation Heating

It may be desirable to increase T_0 to avoid condensation, and to bring local static temperatures up to values at which the viscosity may be reliably estimated. This has a number of collateral consequences, which may be estimated if we assume that $\dot{m}/p_1$ is independent of T_0, and take $\omega = 3/4$. The latter assumption leads to a considerable oversimplification.

(a) D increases as $T_0^{1/4}$ for fixed p_0/p_1 or M_s.

(b) M_s increases as $T_0(\gamma - 1)/4$ for fixed D.

(c) M/Re_* decreases as $T_0^{-1/4}$ for fixed M_s, Re_s/L.

(d) Re_s/L decreases as $T_0^{-(1/2)-\omega}$ for fixed p_1 and M_s.

(e) Re_s/L decreases as $T_0^{-(1/2)-\omega}$ for fixed p_0 and M_s.

VI. TECHNIQUES OF EXPERIMENTAL EVALUATION IN VISCOUS AND MORE RAREFIED REGIMES

At the present date even the experimental picture of free jet structure in the highly viscous regime is not clear, because the viscous effects are at first rather subtle, influencing only those flow properties, such as static temperature and pressure, which are hardest to measure.

A. Impact Pressure Measurements

The key point to recognize in the use of the impact tube in hypersonic flow is that $p_i \simeq \rho^2$ is quite accurately independent of M and T. Hence a viscous effect which greatly increases T but hardly affects ρ or u will not be easily seen in impact pressure data, except through the influence of M and T on the viscous or molecular flow effects on probe readings.

The evaluation of the latter effects in the extended range of M and Re made available by the free jet is a major task in itself, which has been extensively undertaken at the Jet Propulsion Laboratory. Measurements were made using externally chamfered pitot tubes in conjunction with an unbonded-strain-gauge-diaphragm pressure transducer. The geometry of the tubes used was similar, viz.

(a) 10° external chamfer

(b) Ratio of O.D. to I.D. = 1.25

(c) Ratio of length to outside radius = 100.

Pitot tube corrections applicable to the low density, high Mach number flow in the jet were deduced as follows:

The pitot tube data of Ashkenas (1962) (obtained in a conventional low density nozzle flow at M = 4) were used as a starting point for a boot-strap procedure using three geometrically similar pitot tubes; the small region in the free jet between $3.5 \leq M \leq 4.5$ was systematically covered with these three pitot tubes at stagnation pressures ranging from 0.1 mm Hg to 7.0 mm Hg. The impact pressure determined from the corrected pitot tube data was found to be within 2 percent of the Owen and Thornhill values,

over the entire pressure range, and thus the characteristics solution for the axial impact pressure distribution is assumed valid for the flow conditions studied. The pitot tube may then be calibrated over the entire range of Mach numbers available in the jet. Pitot tube correction curves obtained in this manner are shown in Fig. 11. Note that these curves were obtained for integer Mach numbers; linear interpolation between curves was used in reducing data for non-integer Mach numbers. It will be noted in Fig. 11 that the pressures sensed by the pitot tube can range as high as 300 percent of the ideal value calculated from the Rayleigh pitot tube formula.

B. Molecular Beam Methods

A powerful, but subtle, approach to the free-jet diagnostic problem involves the skimming of molecular beams from the jet flow and the determination of the velocity distribution of the beam, as has been done by Bier and Hagena (1963). It is imperative, however, that the "skimming" process be perfect, in the sense of causing no perturbation of the distribution function, and it is hard to prove that a perfect skim has been obtained except in a flow of known properties. A careful boot-strap procedure, involving interative improvements in knowledge of the flow properties and the skimmer operation, seems indicated.

C. Electron Beam Methods

Another attractive possibility, to obtain the local static temperature by the excitation of rotational band spectra of N_2 by an electron beam (Muntz, (1961) is being explored at Berkeley by F. Robben. His preliminary results seem to indicate the necessity of an elaboration of Muntz's theory for the excitation and de-excitation processes. Whether this can be successfully achieved remains to be seen.

VII. CONCLUSIONS

After two years of further study, the proposal that free jets be seriously considered as an alternative type of low density wind tunnel stream seems to be substantiated. Truly impressive extensions of the Mach and

Reynolds number ranges of a tunnel such as that at Berkeley can be obtained, while nearly inviscid flow conditions are maintained. A greater concern with viscous effects arises with pumping systems with lower volumetric capacities and low operating pressure levels, such as that at the Jet Propulsion Laboratory, but it appears likely that the resulting flows will be very useful when fully understood.

The inviscid theory of free jets is in good shape and can be conveniently expressed by simple formulas in the region where $M \geq 5.5$. The theory of slightly viscous flow seems reasonable, but is experimentally unconfirmed.

For implementation of the viscous flow theory and for the reduction of experimental data at very high Mach numbers, better means for estimating viscosity at very low temperatures are urgently required.

Conclusive experimental evidence concerning viscous effects in the jet must involve direct measurement of the Mach number or of such inaccessible quantities as static pressure or temperature. Molecular beam sampling methods look promising, but must be accompanied by conclusive proof of the perfection of the beam-skimming process.

Table 1. Constants for centerline property distributions

γ	x_0/D	x_0'/D	A	C	$x_{min_{2T}}$*	$x_{min_{3T}}$*	Φ
1.67	0.075	0.04	3.26	0.31	2.5D	1.0D	1.365
1.40	0.40	0.13	3.65	0.20	6D	1.0D	1.662
1.2857	0.85		3.96		4D		1.888

*For values of $x > x_{min}$, the two-term or three-term fitting formulas give accuracy within the random scatter of the computer data.

No third term of form $C\frac{x - x_0}{D}^{-3(-1)}$ seems to fit.

REFERENCES

Adamson, T. C., and Nicholls, J. A. (1959). J. Aero/Space Sci. 26, 16-24.

Ames Research Staff (1953). NACA Technical Report 1135.

Ashkenas, H. (1962). JPL CalTech Space Programs Summary 37-15, Vol. 4.

Bier, K., and Hagena, O. (1963). In Rarefied Gas Dynamics (J. Laurmann, ed.), Vol. 1, pp. 478-496, Academic Press, New York.

Bier, K., and Schmidt, B. (1961). Z. angew. Chem. 13, 493-500.

Fenn, J. B., and Deckers, J. (1963). In Rarefied Gas Dynamics (J. Laurmann, ed.), Vol. 1, pp. 497-515, Academic Press, New York.

Hartmann, J., and Lazarus, F. (1941). Phil. Mag. 31, pp. 35-50, Great Britain.

Ko, D. (1964). Univ. Calif. Aero. Sci. Proj. Rept. AS-64-4.

Ladenburg, R., Van Voorhis, C. C., and Winkler, J. (1949). Phys. Rev. 76, 662-677.

Love, E. S., Grigsby, C. E., Lee, L. P., and Woodling, M. J. (1959). NASA TR-R-6.

Maslach, G. J., Willis, D. R., Tang, S., and Ko, D. (1946). This volume, pp._____.

Muntz, E. P. (1961). UTIA Rept. 71.

Owen, P. L., and Thornhill, C. K. (1948). Aero. Res. Council R and M 2616, Great Britain.

Reis, V. H. (1962). Princeton Univ. Mech. Eng. Dept. Rept. FLD-7.

Sherman, F. S. (1963a). In Rarefied Gas Dynamics (J. Laurmann, ed.), Vol. 2, pp. 228-260.

Sherman, F. S. (1963b). Lockheed Missiles and Space Co. Rept. 6-90-63-61.

Sherman, F. S. (1964a). "Some useful approximations for the isentropic flow in supersonic free jets," to appear.

Sherman, F. S. (1964b). Arch. Mech. Stos. 2, 16, 236-248.

Tang, S. (1964). Univ. Calif. Aero. Sci. Proj. Rept. AS-64-3.

Vali, W., and Thomas, G. M. (1962). ARS J. 32, 1114-1115.

Zigan, F. (1962). Z. Naturforsch. 17a, 772-778.

Fig. 1. Inviscid Flow Geometry

$$R = \left\{ r^2 + (x - x_0)^2 \right\}^{1/2}$$

$$\theta = \tan^{-1} r/(x - x_0)$$

Fig. 2. Effect of Entry Geometry on Centerline Mach

Fig. 3. Axial Impact Pressure Distribution

Fig. 4. Radial Mach Number Distribution

Fig. 5. Mach Disc Location

Fig. 6. Impact Pressure behind Mach Disc

Fig. 7. a) Mach Number Perturbation in Air

b) Mach Number-Reynolds Number Relations in Air, p_0/p_1

Fig. 8. Effective Orifice Diameter

Fig. 9. Radial Pitot Pressure Distributions

Fig. 10. Free Jet Operations; $T_0 = 535°R$

Fig. 11. Pitot Tube Corrections

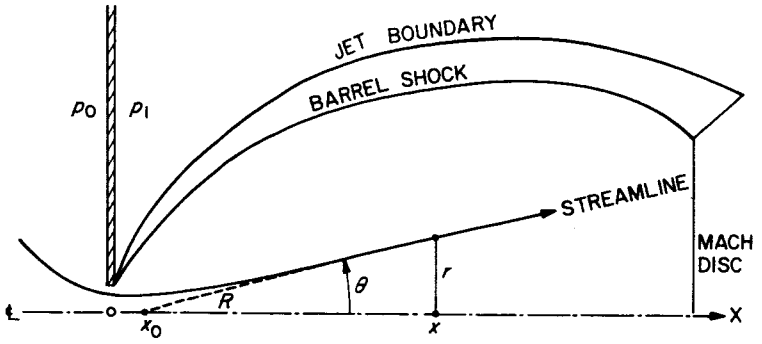

Fig. 1. Inviscid Flow Geometry

$$R = \left\{ r^2 + (x - x_0)^2 \right\}^{1/2}$$

$$\theta = \tan^{-1} r/(x - x_0)$$

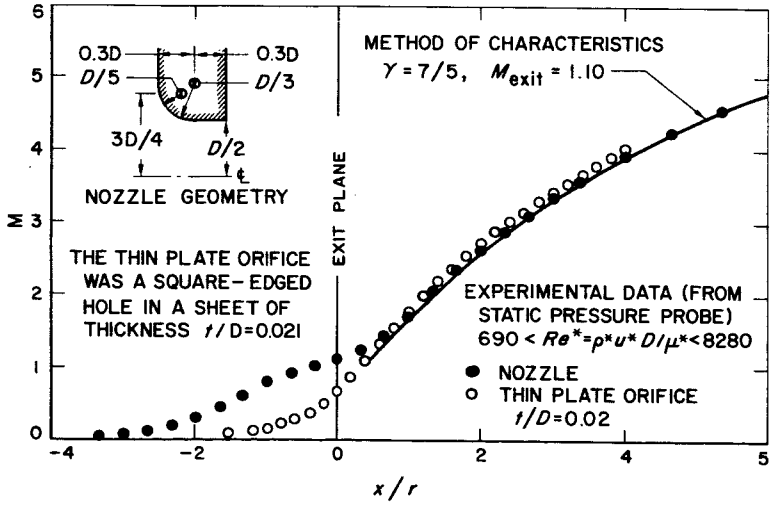

Fig. 2. Effect of Entry Geometry on Centerline Mach

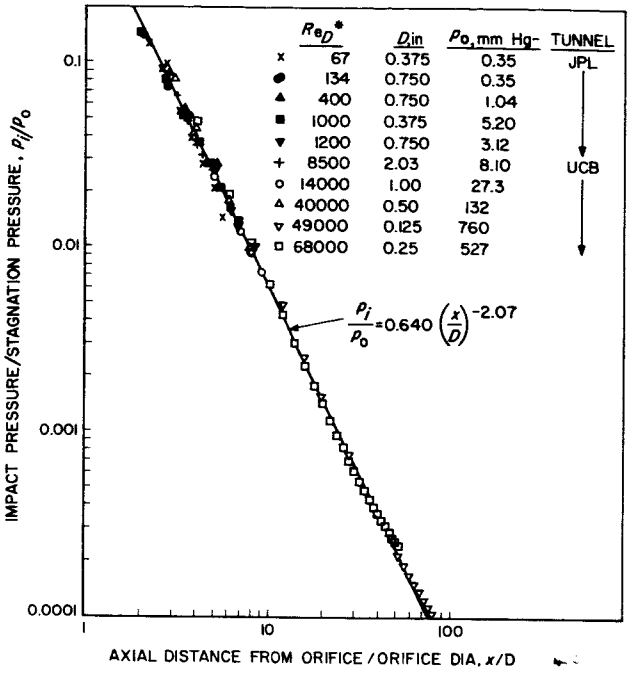

Fig. 3. Axial Impact Pressure Distribution

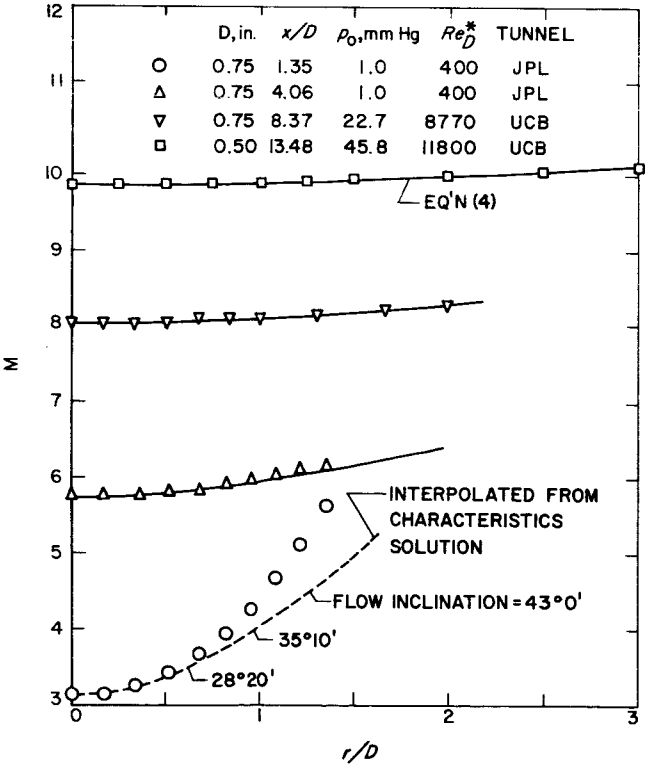

Fig. 4. Radial Mach Number Distribution

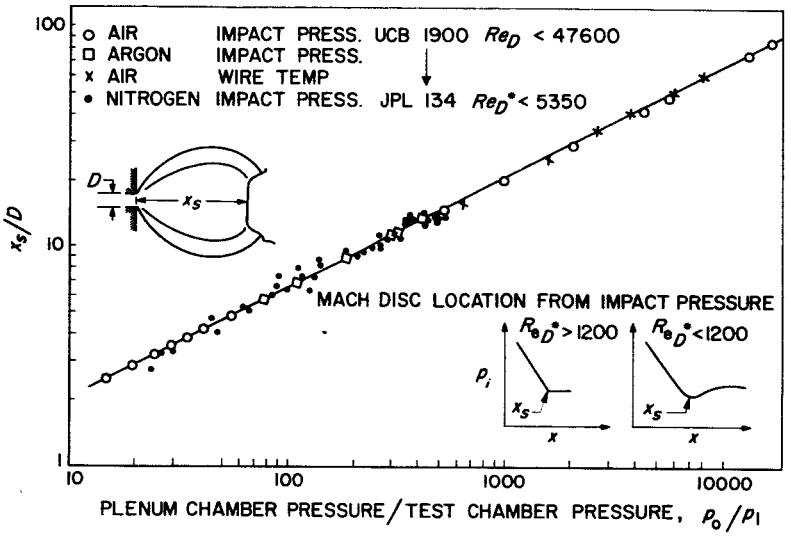

Fig. 5. Mach Disc Location

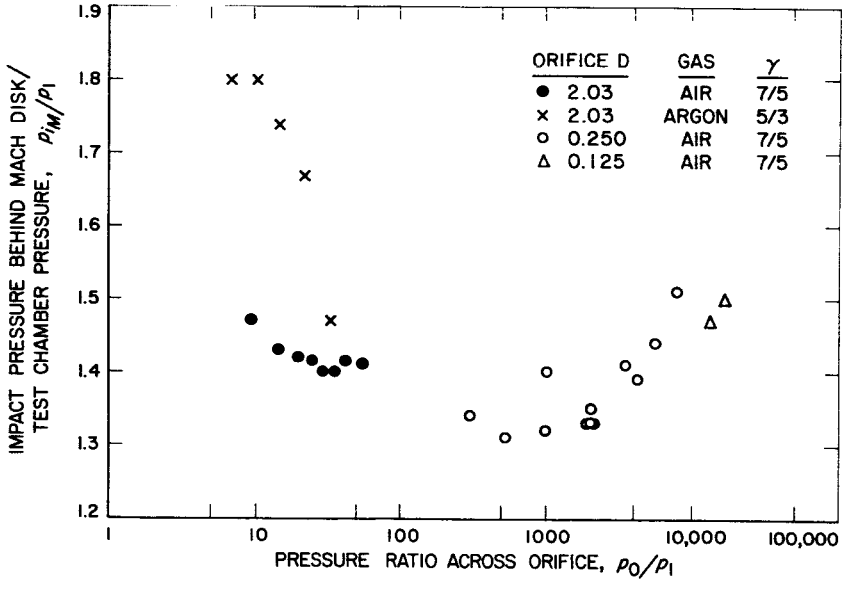

Fig. 6. Impact Pressure behind Mach Disc

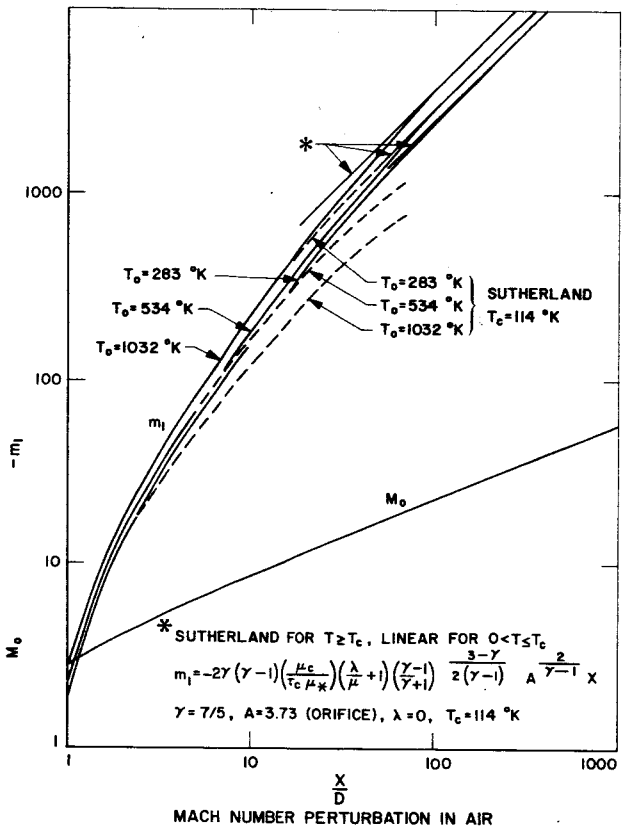

Fig. 7. a) Mach Number Perturbation in Air

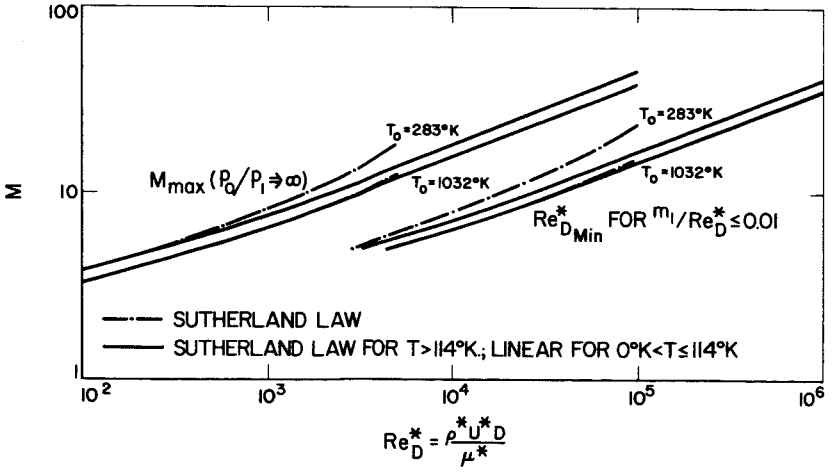

Fig. 7. b) Mach Number-Reynolds Number Relations in Air, p_0/p_1

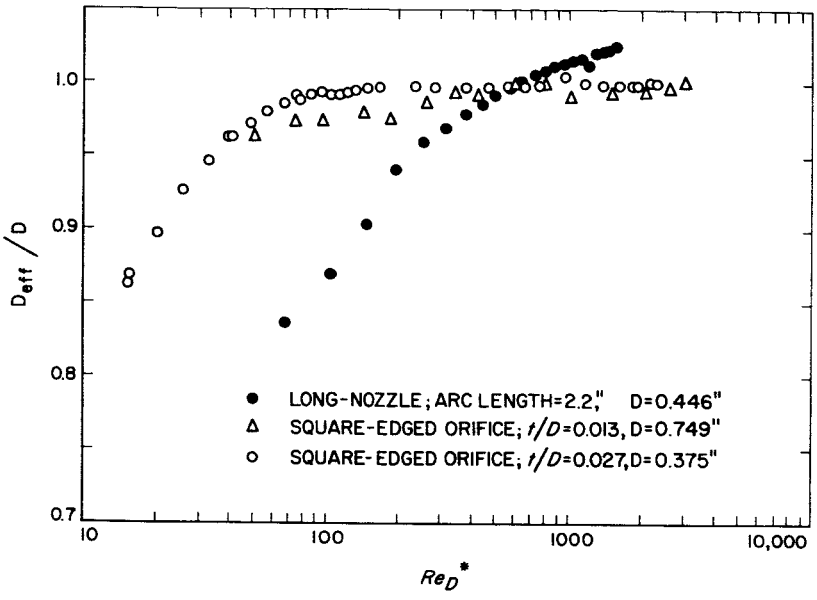

Fig. 8. Effective Orifice Diameter

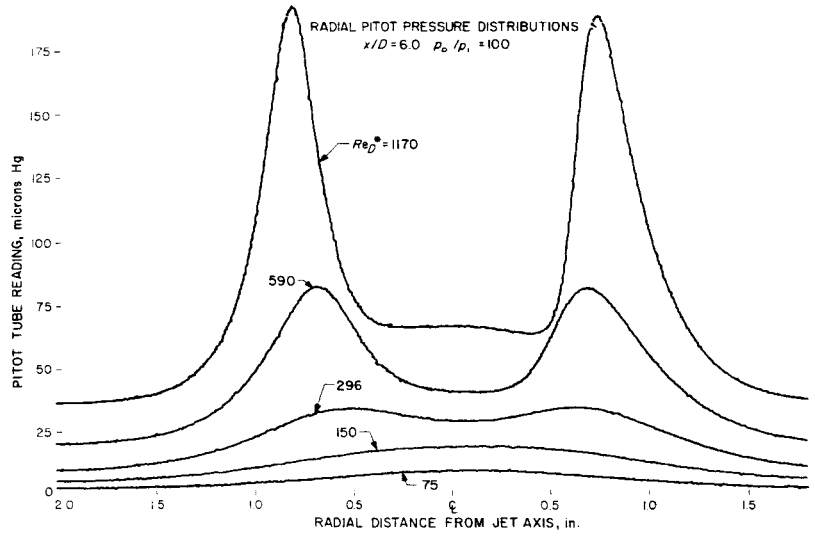

Fig. 9. Radial Pitot Pressure Distributions

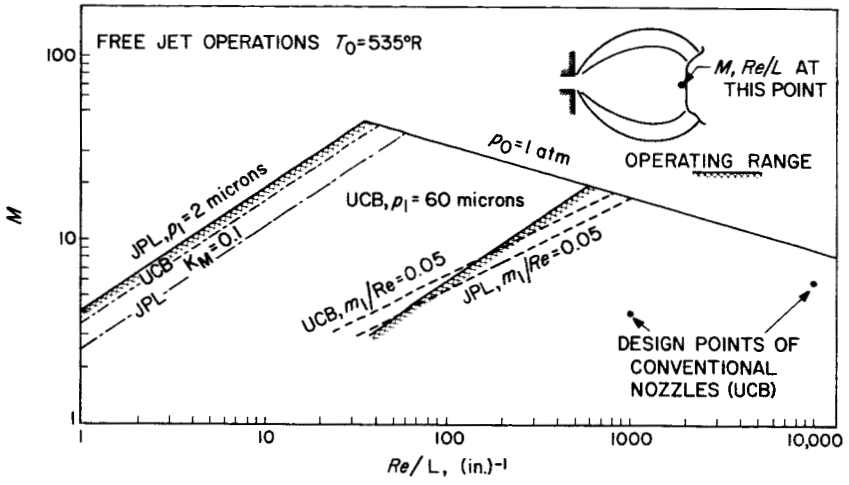

Fig. 10. Free Jet Operations; T_0 = 535°R

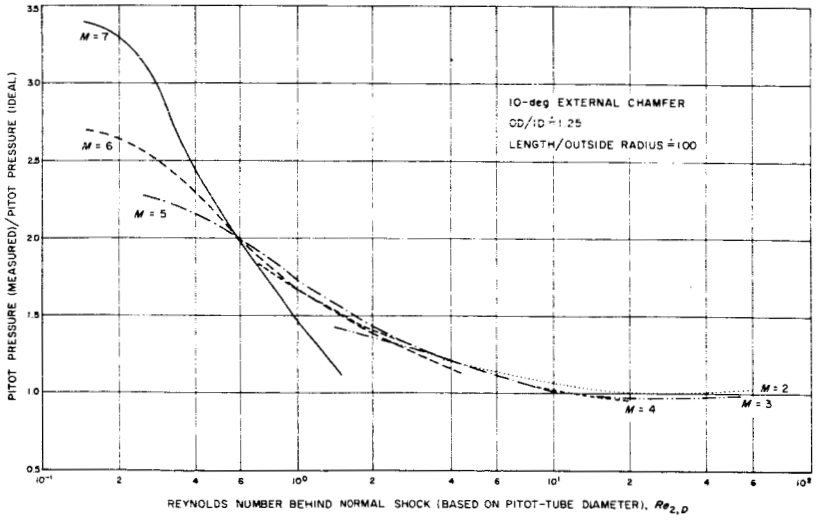

Fig. 11. Pitot Tube Corrections